Silver/alumina for methanol-assisted lean NO$_x$ reduction—On the influence of silver species and hydrogen formation

Marika Männikkö, Xueting Wang, Magnus Skoglundh, Hanna Härelind*

Competence Centre for Catalysis, Chalmers University of Technology, SE-412 96 Gothenburg, Sweden

A B S T R A C T

High low-temperature activity for lean NO$_x$ reduction can be achieved for silver/alumina by using an oxygenated reducing agent. In this system the catalytic reactions, including the H$_2$ formation previously observed during methanol-SCR conditions, are strongly dependent on the composition of surface silver species. With the aim to increase the understanding of the role of supported silver species in combination with the methanol-SCR reactions, catalysts with the same silver loading but different composition of silver species are prepared by utilizing different preparation methods. The supported silver species are characterized by UV–vis spectroscopy and transmission electron microscopy, while the catalytic performance for lean NO$_x$ reduction with methanol is investigated in flow reactor experiments and surface species studied by DRIFT spectroscopy. The results indicate that hydrogen atoms are abstracted mainly from the methyl group during the conversion of surface species formed from methanol. The hydrogen atoms could contribute to reduction of the catalyst or affect the catalytic reactions in other ways, before they react to form H$_2$ or H$_2$O. Here, more H$_2$O is formed over the samples containing more silver nanoparticles. The released hydrogen atoms are suggested to explain the high NO$_x$ reduction at low temperature associated with oxygenated reducing agents, rather than the subsequently formed gaseous H$_2$. Furthermore, the results show that lean NO$_x$ reduction with methanol is determined by silver species in the size range from small silver clusters to small silver nanoparticles (<ca 20 nm). Small silver nanoparticles (<ca 20 nm) are concluded to catalyse formation of N$_2$O. The role of silver ions and small clusters, on the other hand, is suggested to be promotion of N$_2$ formation. The largest silver nanoparticles observed in this study (>ca 20 nm), however, do not have a significant impact on the catalytic reactions. Finally, in order to achieve both high low-temperature activity, as well as high selectivity to N$_2$ a combination of small and somewhat larger silver species are needed.

© 2015 Elsevier B.V. All rights reserved.

1. Introduction

In recent years fuel-efficient engines, operated in oxygen excess, have become increasingly popular, owing to more stringent emissions legislation, increasing oil prices and a general concern for the global climate. Since the conventional three-way catalyst is not active for NO$_x$ reduction in lean conditions other techniques have to be considered. One possibility is hydrocarbon assisted selective catalytic reduction (HC-SCR), where the fuel is used as reducing agent and injected in appropriate amounts into the exhaust system prior to the SCR catalyst. In this context silver/alumina (Ag/Al$_2$O$_3$) catalysts have shown promising results [1–4]. Several preparation

methods have been used [5–11], resulting in different catalytic properties. Particularly important is the silver phase, i.e. Ag$^+$ ions, small clusters (Ag$_n^{m+}$) and nanoparticles, which has been extensively studied [5,7,12–19]. Surface species of NO$_x$ and hydrocarbons have been investigated [20–22] and reaction mechanisms, where partially oxidized hydrocarbons react with adsorbed NO$_x$ species via isocyanates (−NCO) or cyanides (−CN) and possibly amines or ammonia to finally form N$_2$, have been proposed [3,11,22–24], but are still debated. A number of reducing agents have shown promising results, both hydrocarbons [21,25–27] and oxygenates [22,23,28–31]. A challenge for the Ag/Al$_2$O$_3$ catalysts is, however, to achieve high catalytic activity at the low temperatures of lean exhaust gases [32]. One way to improve the low-temperature activity of Ag/Al$_2$O$_3$, is to co-feed hydrogen [4,33,34] together with the reducing agent or to use an oxygenated reducing agent, like ethanol [22,23,28–31]. In the present study methanol is investigated as reducing agent for NO$_x$. Methanol can be produced from renewable sources and is a promising future fuel for mobile applications

Table 1
Silver loading and specific surface area of the prepared samples. Samples with comparable silver loading in bold (ca 4 wt% Ag) and underlined (ca 1 wt% Ag).

Preparation method	Sample designation	Aimed Ag loading (wt%)	Measured Ag loading (wt%)	Specific area[a] (m^2/g)
Sol–gel	SG10	10.0	9.6	180
	SG5	5.0	4.5	212
	SG4	4.1	**4.0**	204
	SG1	1.4	1.4	240
	SG0	0.0	0.0	228
Acid leaching	**LE4**	4.1	**3.8**	194
	LE1	1.4	1.3	210
	LE0	0.0	0.0	230
Physical mixing	**MX4**	4.1	**4.5**	178
	MX3	–	3.0	–
	MX1	1.4	1.6	191
	MX0	0.0	0.0	189
Micro-emulsion	**ME4**	4.1	**4.1**	181
	ME1	1.4	1.2	189
	ME0	0.0	0.0	183

[a] The specific area is calculated by dividing the measured BET area with the weight of the alumina support.

[35]. Recently, we reported on formation of H$_2$ during lean NO$_x$ reduction with methanol [36]. We suggested that this formation of H$_2$ could explain the relatively high NO$_x$ reduction at low temperatures associated with alcohols as reducing agents. Likely, the reason behind the promotional effect of the H$_2$ formed, during SCR with alcohols, would be similar to that of H$_2$ added during SCR with non-oxygenated hydrocarbons. The reason behind this effect is, however, not clear [18,37–45]. One suggestion is that H$_2$ influences the dispersion and chemical state of silver in the Ag/Al$_2$O$_3$ catalyst [18,36,45]. Here, the composition of silver species on the catalyst surface plays an important role. It can be assumed that H$_2$ will affect different silver species to different extent and possibly in different ways, such as reduction and/or agglomeration. This in turn would influence the NO$_x$ reduction, as different silver species are thought to have different roles for the lean NO$_x$ reduction [5,7,14–18]. In this context it is important to understand the influence of the different types of silver species on the catalytic performance of Ag/Al$_2$O$_3$ for lean NO$_x$ reduction. It is, however, difficult to differentiate the influence of a certain type of silver species from the influence of the silver loading of the catalyst, as these are strongly linked together. A high silver loading, for example, implies a high number of large silver agglomerates or nanoparticles, while a catalyst with a low silver content normally has a high dispersion of silver.

In order to investigate exclusively the influence of the types of silver species, catalysts with the same silver loading but with different composition of silver species can be compared. One way to achieve this is to utilize different preparation methods. A preparation method known to result in catalysts with a high dispersion of silver is the sol–gel method including freeze-drying [5,26]. Kannisto et al. showed by XRD, XPS and TEM that the sol–gel method results in a higher proportion of small silver species (i.e. small clusters and ions) compared to conventional impregnation [5]. An alternative technique to prepare catalysts with a high dispersion of silver is by leaching with diluted nitric acid. Using this preparation method She and Flytzani-Stephanopoulos [7], and Yan et al. [8] were able to remove silver particles and weakly bound silver from the surface of Ag/Al$_2$O$_3$ catalysts. By combining the sol–gel method with nitric acid leaching the dispersion of silver could presumably be further increased. For preparation of Ag/Al$_2$O$_3$ with a low dispersion of silver, on the other hand, preparation methods resulting in nanoparticles should be considered. One such method is based on microemulsions, where the size of the prepared nanoparticles is largely determined by the size of the droplets in the microemulsion [46]. Another catalyst preparation method, which has been described recently is physical mixing or ball-milling of γ-Al$_2$O$_3$

together with a silver precursor [9,10]. The authors describe different methods to increase the dispersion of silver, like ball-milling for a fairly long time [9,10]. However, by not following their advice and mixing the ingredients only during a short time, a catalytic material with large silver agglomerates or nanoparticles could be produced.

The present work investigates the role of the composition of supported silver species and the formation of hydrogen for lean NO$_x$ reduction with methanol. The aim is to separate the influence of the composition of silver species from the influence of the silver loading. For this purpose Ag/Al$_2$O$_3$ catalysts are prepared according to different methods, aiming at the same silver loading. The conversion of NO is in focus and the mechanism behind the H$_2$ formation is discussed based on DRIFTS analysis.

2. Experimental methods

2.1. Catalyst preparation

Ag/Al$_2$O$_3$ samples were prepared by different methods in order to create samples with different composition of silver species. Samples were prepared aiming at two different silver loadings, shown in Table 1. In order to achieve a wide variety of silver species a low (1.4 wt% Ag) and a high (4.1 wt% Ag) target silver loading was chosen based on previous results for lean NO$_x$ reduction with methanol [13]. An additional sample was prepared by physical mixing, containing 3 wt% Ag, in order to more clearly be able to differentiate between the effect of silver loading and the types of silver species. As reference γ-Al$_2$O$_3$ samples were prepared according to the same methods. The preparation methods used were sol–gel, acid leaching, physical mixing and microemulsion. The deposition of the powder samples onto cordierite monoliths (diameter 2 cm, length 2 cm, wash-coat 0.5 g) has been described previously [13]. For the DRIFTS studies Ag–Al$_2$O$_3$ (3 wt% Ag, sol–gel), previously described in Ref. [13], and a γ-Al$_2$O$_3$ (sol–gel) sample, were used.

Sol–gel: The sol–gel method including freeze-drying has been described previously [5]. Briefly, a sol was formed by slowly adding diluted nitric acid to an aqueous solution of aluminum isopropoxide and AgNO$_3$. After removal of excess solvent the formed gel was freeze-dried, crushed and calcined in air (600 °C for 6 h). Sol–gel samples containing ca 10 and 5 wt% Ag (Table 1) were prepared as starting material for the acid leaching preparation method.

Acid leaching: Inspired by She and Flytzani-Stephanopoulos [7] and Yan et al. [8], samples were prepared by leaching Ag/Al$_2$O$_3$ in acid. The aim was to remove silver nanoparticles. Sol–gel samples

(SG10 and SG5 in Table 1) were exposed to diluted nitric acid (10% aq.) under vigorous stirring at room temperature for 4 h. Subsequently the aqueous mixture was repeatedly filtered and washed with Milli-Q water. Finally, the samples were freeze-dried and calcined in air (600 °C for 3 h).

Physical mixing: With the goal to produce mainly large silver agglomerates Ag/Al_2O_3 was prepared by physically mixing a silver precursor with γ-Al_2O_3. Ag_2O (Alfa Aesar, 99.99%) and γ-Al_2O_3 (SASOL Puralox SBa-200) were grinded in a mortar for ca 1.5 min in order to create an even distribution. The short time and manual grinding was chosen in order to get a low dispersion of silver, opposite to the work by Petitto and Delahay [10] and Kamolphop et al. [9]. Finally, the mixture was calcined in air (600 °C for 6 h).

Microemulsion: In order to produce Ag/Al_2O_3 with mainly silver nanoparticles, samples were prepared by a microemulsion method, similar to the one used by Tamm et al. [11]. Silver particles were prepared in a water-in-oil microemulsion, where the continuous oil phase consisted of *n*-heptane (Sigma–Aldrich, GC, 99%) with Brij L4 (Sigma–Aldrich, Average Mn ~362) as surfactant. A microemulsion was formed by adding an aqueous solution of $AgNO_3$ (2 wt%) into the oil phase under vigorous stirring. The composition used was 74 wt% *n*-heptane, 20 wt% Brij L4 and 6 wt% $AgNO_3$ solution. While exposing the microemulsion to light for ca 8 h, the formation of silver nanoparticles in the water droplets was followed by UV–vis spectroscopy using a HP/Agilent 8453 UV–vis Spectrophotometer. Subsequently, γ-Al_2O_3 (Sasol Puralox SBa-200) was stirred into the microemulsion. In order to deposit silver particles onto the γ-Al_2O_3 the microemulsion was broken by drop-wise addition of tetrahydrofuran (Sigma–Aldrich) under continuous stirring. The volume of the added tetrahydrofuran was three times the microemulsion volume. After stirring overnight, the suspension was filtered and the filter cake was dried in air at room temperature. The dry powder was finally calcined in air (600 °C for 6 h).

2.2. Characterization and catalytic performance

Quantitative analysis of the silver content of the samples was performed by X-ray fluorescence (XRF) spectroscopy using a PANalytical PW2424 instrument and the software UniQuant 5.0. The specific surface area of the powder samples was determined by nitrogen sorption at −196 °C according to the BET method [47] using a Micromeritics Tristar 3000 instrument. The results are shown in Table 1. Transmission electron microscopy images of the silver containing powder samples were obtained using a JEOL JEM-1200 EX II instrument. Finely ground sample powder was dispersed in ethanol and placed on sample grids (Cu, 3.0 mm, 300 mesh). Furthermore, the silver species in the Ag/Al_2O_3 samples were characterized by UV–vis diffuse reflectance spectroscopy in the range 200–800 nm. The analysis was carried out within 24 h after calcination of the powder samples. The spectrum of a γ-Al_2O_3 sample, prepared in the same way as the corresponding Ag/Al_2O_3 sample, was subtracted from the presented spectra. Spectra were recorded in air at room temperature, using a Varian Cary 5000 UV–vis-NIR spectrophotometer, with Labsphere Spectralon as reference.

The catalytic performance with respect to lean NO_x reduction with methanol was studied for the monolith samples in a continuous flow reactor, described in Ref. [48]. Briefly, feed gases (O_2, H_2, NO and Ar) were introduced into the reactor via separate mass flow controllers (Bronkhorst Hi-Tech). The total flow of 3500 ml/min (GHSV = 33,400 h^{-1}) was balanced with argon. The outlet gas composition was analysed by a gas phase FTIR analyser (MKS Instruments, MultiGas 2030). Temperature programmed reaction experiments were performed according to a previously used procedure [13]. After pre-treatment in 10% O_2 in Ar at 550 °C (30 min), temperature programmed reaction experiments
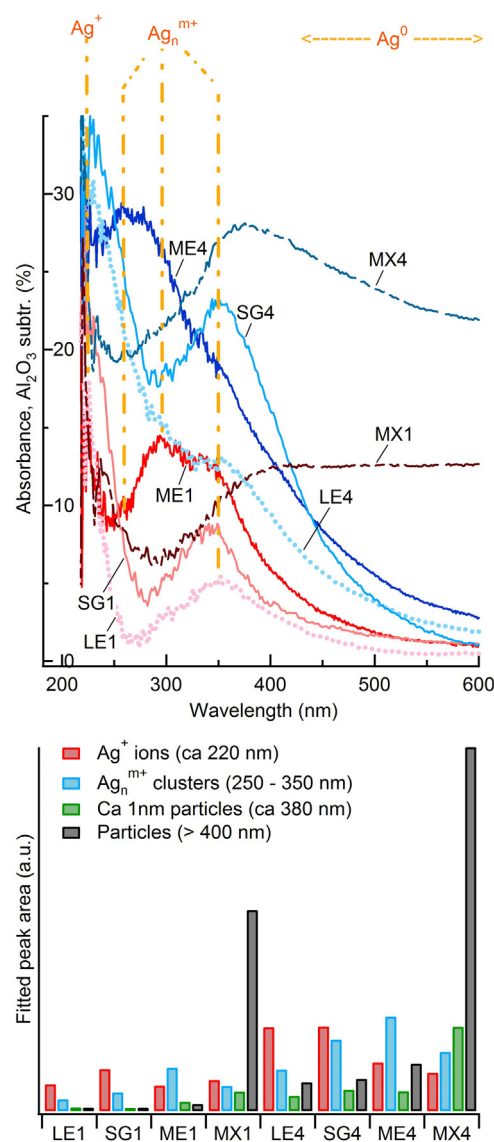
Fig. 1. Characterization of silver species by UV–vis spectroscopy. (a) UV–vis spectra of Ag/Al_2O_3 samples after subtraction of the spectrum for a γ-Al_2O_3 sample prepared by the same method. The spectra were taken after calcination in air (600 °C, 6 h). (b) Area of peaks fitted to the spectra in a. Ag^+ ions (215–220 nm, red), Ag_n^{m+} clusters (250–350 nm, blue), ca 1 nm particles (ca 380 nm, green) and larger nanoparticles (>400 nm, black). For explanation of the sample names see Table 1. (For interpretation of the references to colour in this figure legend, the reader is referred to the web version of this article.)

(550 − 150 °C, 5 °C/min) were carried out in a methanol–SCR gas mixture (500 ppm NO, 1700 ppm methanol and 10% O_2).

Surface species on $Ag-Al_2O_3$ (3 wt% Ag, sol–gel) and γ-Al_2O_3 (sol–gel) were studied by in-situ diffuse reflectance infrared Fourier-transform spectroscopy (DRIFTS) using a BioRad FTS 6000 FTIR spectrometer equipped with a high-temperature reaction cell (Harrick Scientific, Praying Mantis) with KBr windows [49]. Gases were introduced via separate mass-flow controllers (Bronkhorst Hi-Tech) and the outlet gas composition was analysed by mass spectrometry (Balzers QuadStar 420). The sample was first oxidized in the reaction cell at high temperature (10% O_2 at 500 °C, 30 min), where after it was cooled to the reaction temperature in argon. A background spectrum (60 scans, resolution 1 cm^{-1}) was collected in argon, before a step-response experiment was performed in oxygen excess at 260 °C. IR spectra with 1 cm^{-1} spectral resolution were collected with an acquisition frequency of
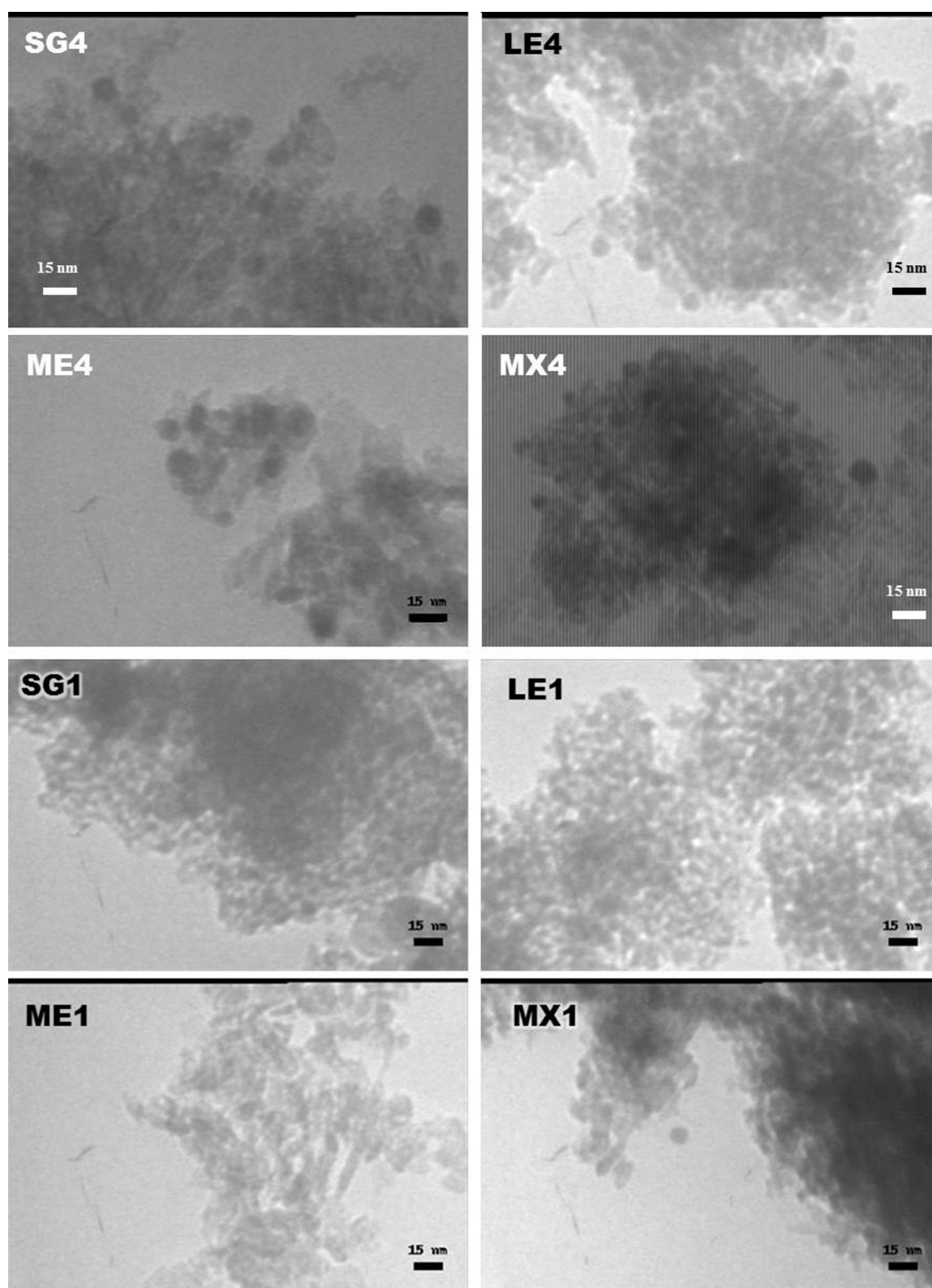
Fig. 2. *Silver particles.* TEM micrographs of Ag/Al$_2$O$_3$ samples with ca 1 and 4 wt% Ag, prepared by different methods, i.e. sol–gel (SG), acid leaching (LE), microemulsion (ME) and physical mixing (MX).

0.1 Hz. NO (500 ppm) or methanol (4000 ppm) was introduced to or removed from the feed after 20 min reaction time, according to the sequence: MeOH, NO + MeOH, NO, NO + MeOH, MeOH, NO + MeOH. The concentration of O$_2$ (10%) was kept constant (Ar bal, total flow 60 ml/min).

3. Results

The specific surface area results for all samples in Table 1 are typical for Ag/Al$_2$O$_3$ [5,7–11,13,26,50]. For the samples prepared by the sol–gel method and acid leaching (where sol–gel samples

are used as starting material) the specific surface area is slightly higher (190–240 m^2/g), compared to the samples based on commercial γ-Al$_2$O$_3$, i.e. the samples prepared by physical mixing and microemulsion (180–190 m^2/g). Furthermore, Table 1 shows that the measured silver content of the samples differs somewhat from the target silver loading (up to ca +/− 15%).

3.1. Characterization

UV–vis spectroscopy was used to characterize the silver species in the prepared samples. Fig. 1a shows the absorbance spectra

of the Ag/Al_2O_3 samples, after subtraction of the spectrum of a γ-Al_2O_3 sample prepared by the corresponding method. The UV–vis spectra in Fig. 1a were deconvoluted and the (summed) areas for the fitted peaks in different wavelength regions are shown in Fig. 1b. All Ag/Al_2O_3 samples show a peak at ca 220 nm, which is attributed to the $4d^{10}$ to $4d^9s^1$ transition of highly dispersed Ag^+ ions [7,14,15,17,51–57]. The amount of silver ions in the different samples is represented by the red bars in Fig. 1b. Furthermore, a peak at ca 350 nm is clearly seen in Fig. 1a for the samples prepared by the sol–gel method and acid leaching, and for the 1% Ag sample prepared by microemulsion at slightly lower wavelength. For the other samples this peak is less obvious owing to overlapping peaks. In addition, the samples prepared by microemulsion show absorbance peaks at ca 250–290 nm, which are not clearly seen for the other samples. Peaks in the wavelength region 270–390 nm are commonly attributed to oxidized silver clusters (Ag_n^{m+}) [7,14,17,52–57]. Although some reports mention reduced or metallic silver clusters (at ca 290–350 nm) [15,56–58], the clusters in the present samples are likely to be in oxidized form, since the samples were calcined in air shortly before the UV–vis analysis. Thus, the above mentioned peaks (at 250, 290 and 350 nm) are assigned to oxidized silver clusters (and their summed areas represented by the blue bars in Fig. 1b). The assignment of the 250 nm peak (for the ME4 sample) is less obvious. However, since it appears at higher wavelengths than Ag^+ and close to the region normally assigned to small silver clusters it is likely to also originate in some type of silver clusters. The difference between the clusters giving absorbance at different wavelengths is likely owing to different size [52,59], effective charge [52] or possibly different shape. Pestryakov et al. [52] differentiates between clusters (Ag_n^{m+}) of different size, i.e. $n < 7$ and ca 1 nm, absorbing light at ca 330–360 nm and 350–380 nm, respectively. The latter are represented by the green bars in Fig. 1b. The highest absorbance above 400 nm is found for the samples prepared by physical mixing (Fig. 1a and the black bars in Fig. 1b). Absorbance bands above 400 nm are commonly attributed to large silver agglomerates or nanoparticles in metallic form and originates in their plasmon resonance [7,14,17,52–54,57,60]. Differences in this wavelength region (>400 nm) have previously been assigned to differences in particle size and shape [61], where larger particles are reported to give band broadening [59] and a shift towards higher wavelengths [62]. Thus, the samples prepared by physical mixing are assumed to have a broad particle size distribution and contain larger particles compared to the other samples.

Transmission electron microscopy (TEM) was used to study the size of the supported silver nanoparticles for Ag/Al_2O_3 prepared by different methods. Care has to be taken when interpreting TEM results when ethanol is used to disperse the Ag/Al_2O_3 samples, since it has been shown to cause agglomeration of silver [63]. However, a relative comparison of the samples should be possible. Fig. 2 shows representative TEM micrographs of the ca 20 images studied for each Ag/Al_2O_3 sample. For the LE4 sample nanoparticles of ca 5–10 nm are observed, while the most common particle size for the SG4 and ME4 samples is ca 5–15 nm, and 5–40 nm for the MX4 sample (Fig. 2). In the present study, also isolated larger particles are observed (up to ca 80 nm) for all 4% Ag samples except for the sample prepared by acid leaching. For the samples with lower silver loading (ca 1 wt% Ag) silver nanoparticles with a size of ca 5–10 nm are observed for the samples prepared by physical mixing and microemulsion (Fig. 2). It is, however, difficult to distinguish any silver particles in the 1% Ag samples prepared by the sol–gel method and acid leaching. If these samples contain any silver nanoparticles they are small ($\leq$ca 5 nm). This is in line with earlier size observations [5,7,17,26,64], where the preparation method was reported to influence the silver particles size [5] and a higher silver loading resulted in larger particles [26,64].
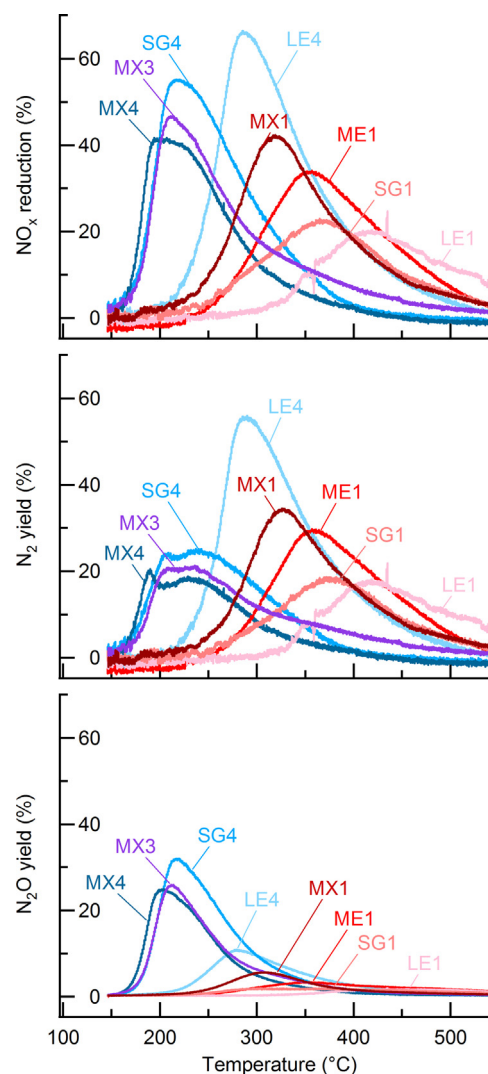
Fig. 3. *Lean NO$_x$ reduction with methanol – influence of silver species.* NO$_x$ reduction and yield of N_2 and N_2O over Ag/Al_2O_3 during cooling ramps in 10% O_2, 1700 ppm CH_3OH, 500 ppm NO, Ar (bal.). Samples containing ca 1 wt% Ag in red and ca 4 wt% Ag in blue. The samples are prepared by different preparation methods, see Table 1.

3.2. NO reduction

The activity and selectivity for lean NO$_x$ reduction with methanol was investigated by flow reactor experiments during cooling from 550 to 150 °C (5 °C/min). Fig. 3 shows the reduction of NO including the formation of N_2 and N_2O for the Ag/Al_2O_3 samples. In addition NO_2 and diminutive amounts of NH_3 and HCN (<20 ppm) are formed (not shown). The NO$_x$ reduction for all samples coincides with the oxidation of methanol (to CO_2, CO and small amounts of formaldehyde, not shown) in accordance with previous results [13]. Fig. 3 shows that the samples with higher silver loading (ca 4 wt% Ag) are active at lower temperature compared to the other samples (with ca 1 wt% Ag), as expected. In addition to the silver loading, also the preparation method affects the active temperature window for the catalysts. The samples prepared by acid leaching are active at higher temperature, compared to the other samples (Fig. 3), while the samples prepared by physical mixing are active at low temperature. Furthermore, the samples containing more silver (ca 4 wt%) show a higher maximum NO$_x$ reduction, compared to the other samples (with ca 1 wt% silver), in accordance with previous results [13]. However, due to high formation of undesirable N_2O (ca 25–35% N_1 yield) and low formation of N_2 (ca 15–25% N_1
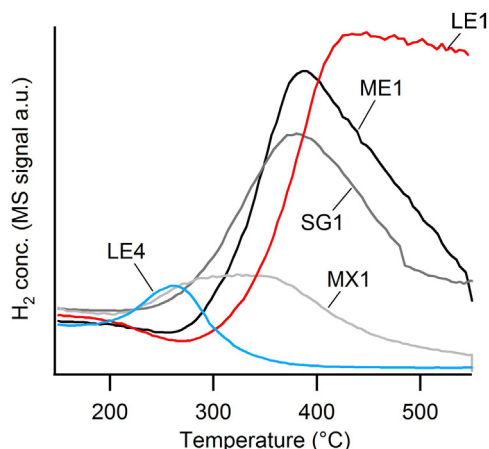
Fig. 4. *Hydrogen formation – influence of silver species.* H_2 formation over Ag/Al_2O_3 (ca 1 or 4 wt% Ag as indicated by the same name) during cooling ramps in 10% O_2, 1700 ppm CH_3OH, Ar (bal.). The samples were prepared by acid leaching (LE), microemulsion (ME), a sol–gel method (SG) and physical mixing (MX).

yield), the selectivity to N_2 is low for the samples active at low temperature (MX4, MX3 and SG4). For the 4 wt% Ag sample prepared by acid leaching (LE4), on the other hand, the selectivity to N_2 is higher (N_2O ca 10% and N_2 ca 55% N_1 yield). In fact, the highest N_2 formation is seen over the LE4 sample. For the 1 wt% Ag samples the selectivity to N_2 is lower for the sample prepared by physical mixing compared to the other samples.

For comparison corresponding results for the γ-alumina samples, prepared according to the same methods as the silver containing samples, can be found in the supporting information. The differences between the γ-alumina samples prepared by different methods are small and more importantly they do not show any obvious connection to the catalytic performance of the silver containing samples.

3.3. Hydrogen formation and surface species

The influence of the composition of silver species for the H_2 formation during methanol oxidation experiments is illustrated in Fig. 4. H_2 formation during cooling ramps (in a flow of 10% O_2 and 1700 ppm methanol in argon) is presented for the samples containing ca 1 wt% Ag and LE4 (Fig. 4). For the other samples with ca 4 wt% Ag no significant amounts of H_2 is observed in the reactor outlet and for all γ-Al_2O_3 samples the H_2 formation occurs at high temperature (not shown). Owing to difficulties in calibrating H_2 for all experiments Fig. 4 shows the MS signal for $m/z = 2$. This implies that the concentration of H_2 for the different samples should not be compared, but only the temperature interval for H_2 formation. The maximum H_2 formation over the samples in Fig. 4 occurs in the following temperature order from low to high temperature: LE4 « MX1 « ME1 ≈ SG1 « LE1. Furthermore, to facilitate a mechanistic discussion regarding the formation of hydrogen from methanol, the main conversion products formed from methanol during methanol-SCR conditions are presented in Fig. 5 for one of the Ag/Al_2O_3 samples (ME1) and the γ-Al_2O_3 sample (ME0) prepared by the same method. The ME1 sample was chosen as an example, since it shows a high formation of H_2, and illustrates that the H_2 formation can be connected to the formation of several carbon containing gas phase species. The concentration of H_2 was analysed by mass spectrometry ($m/z = 2$), but also calculated based on the main gas phase species formed from methanol, which were analysed by FTIR (CO_2, CO, formaldehyde, DME and H_2O). The calculation was performed with the assumption that all incoming hydrogen atoms end up in gas phase. Fig. 5 shows that the cal-
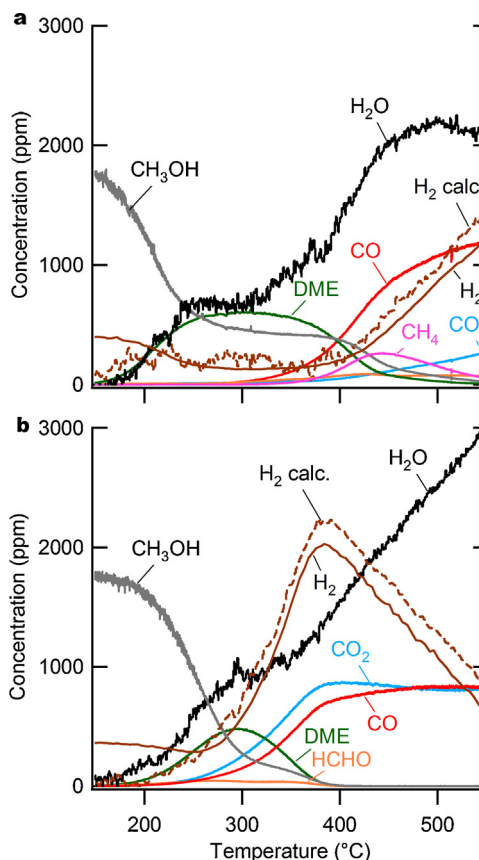
Fig. 5. *Hydrogen formation from methanol.* Methanol conversion over (a) γ-Al_2O_3 (ME0) and (b) Ag/Al_2O_3 with 1 wt% Ag (ME1), prepared by microemulsion, during cooling ramps in 10% O_2, 1700 ppm CH_3OH and Ar (bal.). H_2 analysed by MS (solid line) and calculated from the main conversion products from methanol, measured by FTIR (dashed line).

culated and measured H_2 concentration is similar (except at low temperature, where the $m/z = 2$ signal likely shows fragments of methanol molecules). Fig. 5a shows that the formation of H_2 over the γ-Al_2O_3 sample occurs at high temperature at the same time as CO, CH_4, CO_2 and H_2O are formed. At lower temperature the conversion of methanol to DME is mainly accompanied by formation of H_2O, while only diminutive concentrations of H_2 are observed. Also for the Ag/Al_2O_3 samples in Fig. 5b an increase in the H_2O concentration can be seen at the same temperatures as the formation of DME. As for the γ-Al_2O_3 sample in Fig. 5a, the H_2 formation over the Ag/Al_2O_3 sample in Fig. 5b is accompanied by formation of CO, CO_2 and H_2O, but no CH_4 is formed. At high temperatures more H_2O is formed, on the expense of the H_2 formation (Fig. 5b).

The development of surface species was studied for a Ag/Al_2O_3 sample (3 wt% Ag) by DRIFT spectroscopy, while the inlet gas composition (O_2, methanol and NO) was changed step-wise. The experiment was performed at a temperature (260 °C) were the sample is active for NO_x reduction [13]. As comparison a γ-Al_2O_3 sample was analysed at the same conditions. The pre-oxidized catalyst samples were exposed to a flow of methanol and O_2 for 20 min before NO was introduced. Fig. 6 shows the development of adsorbed carbon containing species in the region 3100–2700 cm^{-1} and changes regarding the hydroxyl groups on the catalyst surface in the region 3850–3600 cm^{-1}. The assignments of the peaks are reported in Table 2. Fig. 6 shows that formate ($CHOO^-$) species are more prominent on the surface of the Ag/Al_2O_3 sample, while more methoxy groups ($-O-CH_3$) are formed on the γ-Al_2O_3 surface. Also the peak at 2745 cm^{-1} assigned to dioxy-methylene ($-O-CH_2-O-$) [49,65] is more abundant for the γ-Al_2O_3 sample compared to
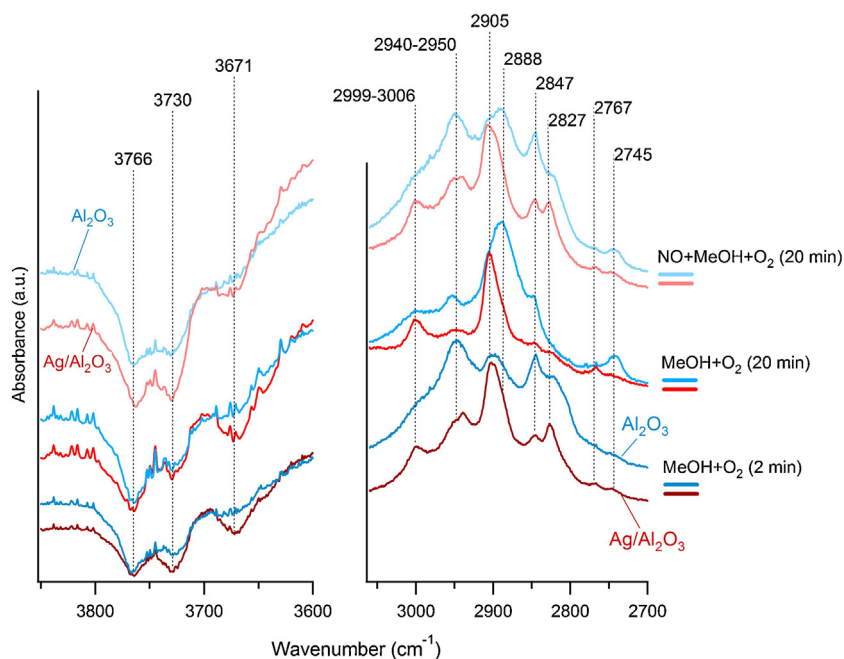
Fig. 6. *Hydroxyl groups and adsorbed carbon species.* DRIFT spectra of Ag/Al$_2$O$_3$ and γ-Al$_2$O$_3$ samples at 260 °C during methanol oxidation and methanol-SCR conditions. Inlet flow: O$_2$ (10%), methanol (4000 ppm), NO (0 or 500 ppm), and argon (bal.). The time mentioned in the figure indicates time passed since the gas composition was changed. The spectra are offset for readability.

the silver containing sample. In the OH region disappearance of OH groups, resulting in negative absorption bands at 3766, 3730 and 3671 cm^{-1}, are observed for both samples upon exposure to methanol. The negative band at 3671 cm^{-1} is, however, somewhat more pronounced for the Ag/Al$_2$O$_3$ sample compared to the γ-Al$_2$O$_3$ sample. Later when NO is introduced to the feed all negative OH bands grow deeper for both samples. The change for the band at 3730 cm^{-1} is, however, more extensive.

Absorption peaks at 2250 and 2236 cm^{-1} are observed for both the Ag/Al$_2$O$_3$ and the γ-Al$_2$O$_3$ sample, and assigned to adsorbed isocyanate (−NCO) species. For the Ag/Al$_2$O$_3$ sample a small peak is observed at 2154 cm^{-1}, assigned to adsorbed cyanide (−CN) species. Fig. 7 shows the development of the −NCO (i.e. the sum of the peaks at 2250 and 2236 cm^{-1}) and –CN species over Ag/Al$_2$O$_3$ during the step-response experiment. Small amounts of −NCO and even smaller amounts of −CN species are formed when NO is present in the feed. When methanol is removed from the feed (i.e. in the presence of only NO and O$_2$) the number of −NCO species

increases, while the number of −CN species decreases. Also a small decrease in other adsorbed carbon containing species is observed at this time. When methanol is re-introduced to the feed (at ca 50 min in Fig. 7) the −NCO peaks rapidly increase and subsequently decrease. When NO is removed from the flow (at ca 80 min) the −NCO peaks decrease further, but return to the previous level when NO is introduced to the flow again (at ca 100 min in Fig. 7).

4. Discussion

The deviation from the target silver loading (up to ca+/−15%) for the samples in Table 1 is considered to be of minor importance for the NO$_x$ reduction, compared to the influence of the preparation method. For example the NO$_x$ reduction over both MX4 (4.5% Ag) and MX3 (3.0% Ag), occurs at lower temperature compared to LE4 (3.8% Ag). These results clearly show that the influence of the composition of silver species is more important than the influence of the silver loading.

Table 2
Assignment of absorption bands in DRIFTS measurements during methanol oxidation and methanol-SCR conditions.

Wavenumber (cm^{-1})	Surface species	Reference
3766	Hydroxyl	[49,76,77]
3730	Hydroxyl	[49,76–78]
3671	Hydroxyl	[49,76,77]
2999-3006	Formate	[16,21,72]
2955	Methoxy	[49,67]
2942	Methoxy or methanol	[49]
2905	Formate	[16,21,49,69]
2888	Methoxy	[49]
2847	Methoxy	[49,67,69,79]
2827	Methoxy or methanol	[49]
2767	Dioxy-methylene	[49,65]
2745	Dioxy-methylene	[49,65]
2250	NCO	[72,73]
2236	NCO	[16,72–74]
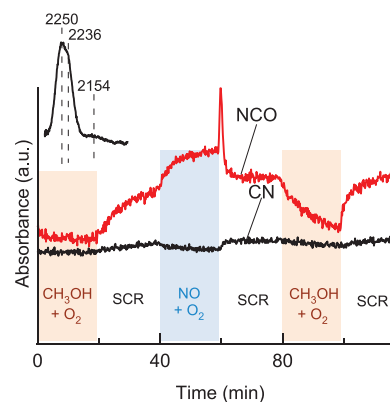
Fig. 7. *Isocyanate and cyanide species.* Development of NCO (2250 and 2236 cm^{-1}) and CN (2154 cm^{-1}) adsorbates during a step-response experiment over Ag/Al$_2$O$_3$ (3 wt% Ag) at 260 °C. Inlet flow: O$_2$ (10%), methanol (0 or 4000 ppm), NO (0 or 500 ppm), and argon (bal.).

4.1. Low-temperature activity

Ag/Al_2O_3 with high silver content is thought to contain a large number of silver nanoparticles [14,18,26]. Previously, Ag/Al_2O_3 with a high silver content has shown activity for NO_x reduction at low temperature [13]. Thus, it has been assumed that nanoparticles or large silver species promote low-temperature activity. Here, this assumption is investigated in further detail by studying samples of comparable silver loading, prepared by different methods resulting in different composition of silver species. The NO_x reduction of the as prepared samples appear in Fig. 1 in the following order, from low to high temperature: MX « ME < SG « LE. The order is the same for the analysed samples with ca 1 wt% Ag as for those with ca 4 wt% Ag. Could this temperature order be explained by the types of silver species in the samples? We search for supporting evidence in the results from the characterization of silver species.

First, we focus on evidence of large silver nanoparticles and compare it to the temperature for NO_x reduction. According to the characterization by UV–vis spectroscopy (Fig. 1) and TEM (Fig. 2) the samples prepared by physical mixing contain a significantly higher number of large silver particles (>ca 20 nm) compared to the other samples. If these large silver nanoparticles would be responsible for the temperature when the NO_x reduction occurs, we could expect that the NO_x reduction over the physically mixed samples would start at much lower temperature compared to the other samples. This is however not the case. The NO_x reduction over the mixed samples does indeed start at lower temperature compared to the other samples, but not at very much lower temperature. Thus, we suggest that the large silver particles (>ca 20 nm) do not (alone) determine the temperature for NO_x reduction.

Secondly, evidence of somewhat smaller silver species (small particles and silver clusters) are discussed and compared to the temperature for NO_x reduction. In the UV–vis analysis these small silver species absorb light in the region ca 250–450 nm (Fig. 2). The amount of small silver species for the samples in Fig. 1 shows a relation to the temperature for NO_x reduction in Fig. 3. In other words a high content of these rather small silver species in a sample promotes NO_x reduction at low temperature. The wavelength region where these small species absorb light is mainly represented by the blue and green bars in Fig. 1b, representing small ($n < 7$) silver clusters and small (ca 1 nm) silver nanoparticles, respectively [52]. However, also peaks at ca 400–450 nm, likely originating in somewhat larger silver nanoparticles (<ca 20 nm), show a similar trend.

Finally, it should be noted that the abundance of silver ions (red bars in Fig. 1b) does not show similarities with the trends for the temperature for NO_x reduction. To summarize, it is most likely not only one type/size of silver species which influences the temperature for NO_x reduction, but several types of small ($n < 7$) silver clusters [52], and/or small silver particles (<ca 20 nm). This, however, excludes large silver nanoparticles (>ca 20 nm) and single silver ions.

4.2. Selectivity to N_2

Small oxidized silver clusters (Ag_n^{m+}) and silver ions (Ag^+) are thought to be important for the lean NO_x reduction and selectivity to N_2 [5,14,66]. Large silver species/nanoparticles, on the other hand, are commonly accepted to enhance N_2O formation [3,16]. Here, these assumptions are examined in detail by studying samples of comparable silver loading, but with different composition of silver species.

The highest formation of N_2 is seen in Fig. 3 for the 4% Ag sample prepared by acid leaching (LE4). The reason behind should be sought in the silver species present in high amounts and/or the composition of silver species. The UV–vis analysis in Fig. 1 shows

high amounts of silver ions in the LE4 sample, however, not higher than in the sample prepared by the sol–gel method (SG4). Since the SG4 sample shows lower N_2 formation (Fig. 3), high amounts of silver ions cannot alone explain the high formation of N_2 over LE4. The explanation should instead be sought in the composition of silver species. Remarkable for the LE4 sample, according to the UV–vis analysis in Fig. 1, is the combination of high amounts of silver ions and low amounts of large silver species.

Another advantage with the LE4 sample, compared to the other 4% Ag samples, is the low N_2O formation. For the 1% Ag samples the N_2O formation is even lower, but also the N_2 formation is lower than for the 4% Ag samples. The selectivity to N_2 is, however, in general lower for the samples containing more silver (ca 4 wt% Ag) compared to those with lower silver loading (ca 1 wt% Ag). For the MX1 and LE4 samples, however, the selectivity to N_2 is approximately the same, even if their silver loading is significantly different (1.6 and 3.8 wt% Ag). For LE4 the selectivity to N_2 is above assumed to be influenced by the composition of silver species. Thus, an explanation for the selectivity for MX1 should also be found in the composition of silver species. Obviously the silver species resulting in the absorbance at high wavelengths (>ca 450 nm in Fig. 1) for the MX1 sample cannot have a decisive impact. Otherwise the NO_x reduction activity over MX1 would be very low and the N_2O formation high. Thus, the explanation has to be, also in this case, a proper combination of small silver species (mainly ions for MX1) and somewhat larger silver species (i.e. small nanoparticles). Likewise, the lower N_2 formation for the SG4, MX3 and MX4 samples compared to LE4, could be explained by a less suitable composition of silver species. Instead high amounts of N_2O is formed (Fig. 3), which can be connected to the high number of small silver nanoparticles in these samples (Fig. 1). Thus, a combination of high amounts of small silver species (i.e. ions and/or small clusters) and low amounts of nanoparticles (favouring the conversion to N_2O) are suggested to be beneficial for a high formation of N_2.

To summarize, the results indicate that (small) silver nanoparticles result in formation of N_2O. Small silver species (ions and clusters), on the other hand, do not seem to promote formation of N_2O. Moreover, high activity for NO_x reduction with a high selectivity to N_2 is achieved at a suitable composition of silver species, i.e. a high number of small silver species (ions and small clusters) and a low number of large silver species (i.e. small nanoparticles). Again, as was suggested for the temperature dependence above, the large silver nanoparticles absorbing light at high wavelengths (>450 nm in Fig. 1) do not have a significant influence on the selectivity of the catalytic reactions.

4.3. Hydrogen formation and surface reactions

The influence of the composition of silver species on the formation of H_2 during methanol oxidation conditions is illustrated in Fig. 4. The concentration of H_2 in the outlet is different for the samples containing ca 1 wt% Ag (LE1, SG1, ME1, MX1). The temperature order for the 1% Ag samples follows the size order of the silver species with one exception. SG1 contains less large silver species than ME1 and is thus expected to give H_2 formation at higher temperature. The reason why the temperature order is the opposite is not clear and experimental difficulties cannot be ruled out. The apparent H_2 formation over LE4 occurs at lower temperature compared to the samples with lower silver loading, in accordance with previous results [36]. For the other 3–4% Ag samples no H_2 was observed in the reactor outlet. For these samples all H_2, which possibly has been formed, is oxidized to H_2O. This indicates that large silver species/particles contribute to the oxidation to H_2O.

H_2 and H_2O are thought to be formed from the hydrogen atoms in methanol, i.e. when methanol is converted to DME, HCHO, CH_4, CO and CO_2, as illustrated for the ME0 and ME1 samples in Fig. 5.

In Fig. 6 adsorbed carbon species and hydroxyl groups on Ag/Al$_2$O$_3$ (3 wt% Ag) and γ-Al$_2$O$_3$ are compared during methanol oxidation and methanol-SCR conditions at 260 °C. Fig. 6 shows that more methoxy groups are formed on the γ-Al$_2$O$_3$ sample, while more formates are present on Ag/Al$_2$O$_3$ at the present temperature. When methanol is adsorbed on the catalyst surface in the form of methoxy groups (−O−CH$_3$), hydrogen atoms are released and thought to either react with −OH groups to form H$_2$O [67,68] or adsorb on the surface at the same time as the methoxy groups may form hydrogen bonds to adjacent −OH groups [69]. Both these mechanisms can explain the negative peaks formed in the OH stretching region in Fig. 6 when methanol is adsorbed. However, since significantly more H$_2$O than H$_2$ is formed at this temperature (260 °C) in Fig. 5a, the formation of H$_2$O from hydrogen atoms (from methanol) and -OH groups seems to be dominating. Moreover, DME (CH$_3$−O−CH$_3$), which is formed (at 260 °C) in Fig. 5a over γ-Al$_2$O$_3$, has been suggested to be formed from methoxy groups reacting with incoming methanol [65,68]. This reaction also results in formation of an −OH group, which could bind to the surface or react with hydrogen atoms to form H$_2$O. Hence, the formation of methoxy groups or DME does not seem to result in any significant formation of hydrogen atoms on the surface or gas phase H$_2$.

Furthermore, the methoxy groups are thought to lose hydrogen atoms and form dioxy-methylene (−O−CH$_2$−O−) and formates (CHOO$^−$) [49,65]. These hydrogen atoms could react and form gas phase H$_2$ or H$_2$O, or result in reduction of the catalyst surface [65]. The dioxy-methylene could leave the surface as formaldehyde (HCHO) [65], while the formates are thought to contribute to the formation of CO [49,65,69] and/or CO$_2$ [65,68], with accompanying formation of H$_2$O [65,69] or −OH groups [65]. This is supported by the results in the present work. The presence of formates on the Ag/Al$_2$O$_3$ sample in Fig. 6 is reflected in the higher formation of CO$_2$ and CO over Ag/Al$_2$O$_3$ at the present temperature (260 °C), compared to over γ-Al$_2$O$_3$ [13]. At low temperatures, however, it is more likely that CO and especially CO$_2$ are formed over the supported silver species. This can be concluded based on the results in Fig. 5b, where more CO and CO$_2$ is formed at low temperatures for the Ag/Al$_2$O$_3$ sample, compared to the γ-Al$_2$O$_3$ sample in Fig. 5a. In addition, for Ag/Al$_2$O$_3$ samples with higher silver loading even more CO$_2$ is formed at low temperatures [13]. These results are in accordance with previous suggestions for HC-SCR reactions on Ag/Al$_2$O$_3$, which include oxidation of hydrocarbons to CO$_x$ and H$_2$O over supported silver particles [3,16]. The formation of H$_2$ over supported silver species, can however not be ruled out. Nagy et al. [70] describes a mechanism for silver catalysts where formaldehyde is formed at the same time as H$_2$ or H$_2$O, where the formaldehyde could subsequently be oxidized to CO or CO$_2$ (possibly explaining the small amounts of formaldehyde observed here). In addition, Matyshak et al. [71] mention that hydrogen atoms released during the reaction of methanol over alumina, could form H$_2$ over supported copper species. Possibly this could occur also for silver. Owing to the oxidizing character of silver nanoparticles, however, the H$_2$ formation over supported silver can be assumed to be more likely over small silver species.

After adsorption of methanol and its further reaction on the catalyst surface, resulting in hydrogen formation, the carbon containing surface species are thought to react with adsorbed nitrogen containing species during the lean NO$_x$ reduction over Ag/Al$_2$O$_3$. Here −NCO species are reported to be an important intermediate [3,72–74]. If some of the formed carbon containing surface species contribute to a higher extent to the formation of −NCO, than the others, can, however, not be determined based on the present experiments. While formation of −NCO species are thought to be important for the NO$_x$ reduction, Ag$^+$CN species are suggested to block the active sites [74], owing to the fact that the conversion of −CN to −NCO is slow [72]. The blocking Ag$^+$CN species are, however,

easily converted to −NCO species in the presence of H$_2$ [40]. Thus, as suggested by Chansai et al. [74], H$_2$ formed from methanol could have a similar effect. Fig. 7 shows the development of −NCO and −CN species on Ag/Al$_2$O$_3$ (3 wt% Ag) during a step-response experiment at 260 °C. During methanol-SCR conditions −NCO species are formed on the Ag/Al$_2$O$_3$ surface (Fig. 7), while only diminutive amounts of −CN are observed. Moreover, during NO oxidation conditions (NO + O$_2$) in Fig. 7 the −NCO species build up. −NCO species are thought to be hydrolysed by H$_2$O–NH$_3$ or amines [16,72,75], during NO oxidation conditions, however, the reaction cannot proceed owing to lack of H$_2$O. When methanol is again introduced to the flow (at ca 60 min in Fig. 7) the number of −NCO species rapidly increases for a short period of time. This can be explained by the build-up of adsorbed NO$_x$ species during the NO oxidation step. When methanol is introduced, they rapidly react with surface species formed from the incoming methanol and form −NCO. The −NCO species in turn are consumed in the reaction with H$_2$O (formed during the oxidation of methanol), which is thought to result in formation of amines or NH$_3$ [16,72,75]. Here, however, no amines or ammonia were observed. Nevertheless, they could have been formed and rapidly reacted further before we were able to detect them. The amines and NH$_3$ are thought to participate in the NO$_x$ reduction in a similar manner as during NH$_3$-SCR, i.e. forming N$_2$ in reactions with mainly adsorbed NO$_x$ species. A short period of time after the start of the methanol-SCR step, the adsorbed and gas phase species levels out and reaches approximately the same amount as during the previous methanol SCR step. Later, when NO is removed from the flow (at ca 80 min in Fig. 7) the −NCO species decrease. Slowly decreasing concentrations of NH$_3$ during this time could be an indication of that the −NCO species here are consumed in reactions forming NH$_3$.

To summarize the investigated parts of the methanol-SCR reactions, it can be concluded that hydrogen atoms are released and −NCO species formed. The hydrogen atoms, mainly abstracted from the methyl group, can bind to the catalyst surface, where they can contribute to for instance reduction of silver, before they react to form H$_2$ or H$_2$O, which in turn could occur either on the alumina support or on the supported silver species. Thus, when H$_2$O is observed in the reactor outlet, hydrogen atoms may have been present on the surface long enough to affect the oxidation state of silver or the catalytic reactions in other ways.

5. Concluding remarks

Silver/alumina catalysts were prepared according to different methods, resulting in different composition of silver species. The results show that the lean NO$_x$ reduction with methanol at low temperature is determined by silver species in the size range: small silver clusters (Ag$_n^{m+}$, $n < 7$) to small silver nanoparticles (<ca 20 nm). The results support earlier suggestions that silver nanoparticles catalyse formation of N$_2$O. Interestingly, however, it is only rather small nanoparticles that are of importance (<ca 20 nm). The largest silver nanoparticles observed in this study (>ca 20 nm), present mainly in the samples prepared by physically mixing alumina with a silver precursor, do not have a significant impact on the catalytic reactions. The role of small silver species (ions and small clusters), on the other hand, is suggested to be promotion of N$_2$ formation, while they do not promote formation of N$_2$O. Furthermore, the composition of silver species on the alumina surface is important for achieving a high selectivity to N$_2$. The results show that a high number of small silver species (ions and small clusters) is beneficial for a high N$_2$ formation. However, in order to achieve both high low-temperature activity, as well as high selectivity to N$_2$ a combination of small and somewhat larger silver species are needed.

Furthermore, possible mechanisms for hydrogen formation from methanol are discussed based on DRIFTS results and related to formed gas phase species. Hydrogen atoms are thought to be abstracted in particular from the methyl group during the conversion of surface species formed from methanol. The hydrogen atoms can contribute to reduction of the catalyst or affect the catalytic reactions in other ways, before they react to form H_2 or H_2O. The results indicate that large silver species promote the formation of H_2O. The released hydrogen atoms could explain the high NO_x reduction at low temperature associated with oxygenated reducing agents, rather than the subsequently formed gaseous H_2. It can hence be understood why a high low-temperature activity during methanol-SCR conditions is seen also when the outlet gas composition contains more water than H_2.

Acknowledgements

Appendix A. Supplementary data

Supplementary data associated with this article can be found, in the online version, at http://dx.doi.org/10.1016/j.apcatb.2015.06.002

References

[1] P. Granger, V.I. Parvulescu, Chem. Rev. 111 (2011) 3155–3207.
[2] F. Klingstedt, K. Arve, K. Eranen, D.Y. Murzin, Acc. Chem. Res. 39 (2006) 273–282.
[3] R. Burch, J.P. Breen, F.C. Meunier, Appl. Catal. B 39 (2002) 283–303.
[4] R. Burch, Catal. Rev. Sci. Eng. 46 (2004) 271–333.
[5] H. Kannisto, H.H. Ingelsten, M. Skoglundh, J. Mol. Catal. A: Chem. 302 (2009) 86–96.
[6] E. Seker, J. Cavataio, E. Gulari, P. Lorpongpaiboon, S. Osuwan, Appl. Catal. A 183 (1999) 121–134.
[7] X. She, M. Flytzani-Stephanopoulos, J. Catal. 237 (2006) 79–93.
[8] Y. Yan, Y.B. Yu, H. He, J.J. Zhao, J. Catal. 293 (2012) 13–26.
[9] U. Kamolphop, S.F.R. Taylor, J.P. Breen, R. Burch, J.J. Delgado, S. Chansai, C. Hardacre, S. Hengrasmee, S.L. James, ACS Catal. 1 (2011) 1257–1262.
[10] C. Petitto, G. Delahay, Catal. Lett. 142 (2012) 433–438.
[11] S. Tamm, H.H. Ingelsten, A.E.C. Palmqvist, J. Catal. 255 (2008) 304–312.
[12] L.E. Lindfors, K. Eranen, F. Klingstedt, D.Y. Murzin, Top. Catal. 28 (2004) 185–189.
[13] M. Männikkö, M. Skoglundh, H. Härelind, Top. Catal. 56 (2013) 145–150.
[14] K.A. Bethke, H.H. Kung, J. Catal. 172 (1997) 93–102.
[15] K. Shimizu, J. Shibata, H. Yoshida, A. Satsuma, T. Hattori, Appl. Catal. B 30 (2001) 151–162.
[16] F.C. Meunier, J.P. Breen, V. Zuzaniuk, M. Olsson, J.R.H. Ross, J. Catal. 187 (1999) 493–505.
[17] N. Bogdanchikova, F.C. Meunier, M. Avalos-Borja, J.P. Breen, A. Pestryakov, Appl. Catal. B 36 (2002) 287–297.
[18] M. Richter, U. Bentrup, R. Eckelt, M. Schneider, M.M. Pohl, R. Fricke, Appl. Catal. B 51 (2004) 261–274.
[19] K. Arve, K. Svennerberg, F. Klingstedt, K. Eranen, L.R. Wallenberg, J.O. Bovin, L. Capek, D.Y. Murzin, J. Phys. Chem. B 110 (2006) 420–427.
[20] M.M. Azis, H. Harelind, D. Creaser, Catal. Sci. Technol. 5 (2015) 296–309.
[21] H. Harelind, F. Gunnarsson, S.M.S. Vaghefi, M. Skoglundh, P.A. Carlsson, ACS Catal. 2 (2012) 1615–1623.
[22] S. Kameoka, Y. Ukisu, T. Miyadera, Phys. Chem. Chem. Phys. 2 (2000) 367–372.
[23] H. He, X.L. Zhang, Q. Wu, C.B. Zhang, Y.B. Yu, Catal. Surv. Asia 12 (2008) 38–55.
[24] K. Eranen, F. Klingstedt, K. Arve, L.E. Lindfors, D.Y. Murzin, J. Catal. 227 (2004) 328–343.
[25] K. Eränen, L.-E. Lindfors, A. Niemi, P. Elfving, L. Cider, Influence of hydrocarbons on the selective catalytic reduction of NO_x over $Ag/Al2O3$ – laboratory and engine tests, SAE Int. Paper #: 2000-01-2813 (2000), http://dx.doi.org/10.4271/2000-01-2813

[26] H. Kannisto, K. Arve, T. Pingel, A. Hellman, H. Harelind, K. Eranen, E. Olsson, M. Skoglundh, D.Y. Murzin, Catal. Sci. Technol. 3 (2013) 644–653.
[27] E.F. Iliopoulou, A.P. Evdou, A.A. Lemonidou, I.A. Vasalos, Appl. Catal. A 274 (2004) 179–189.
[28] R. da Silva, R. Cataluna, A. Martinez-Arias, Catal. Today 143 (2009) 242–246.
[29] T. Miyadera, Appl. Catal. B 2 (1993) 199–205.
[30] W.L. Johnson, G.B. Fisher, T.J. Toops, Catal. Today 184 (2012) 166–177.
[31] J.A. Pihl, T.J. Toops, G.B. Fisher, B.H. West, Catal. Today 231 (2014) 46–55.
[32] M.V. Twigg, Catal. Today 163 (2011) 33–41.
[33] S. Satokawa, Chem. Lett. 29 (2000) 294–295.
[34] J. Shibata, K. Shimizu, S. Satokawa, A. Satsuma, T. Hattori, Phys. Chem. Chem. Phys. 5 (2003) 2154–2160.
[35] G.A. Olah, A. Goeppert, G.K.S. Prakash, Beyond Oil and Gas: The Methanol Economy, 2nd ed., Wiley-VCH, Weinheim, 2009.
[36] M. Männikkö, M. Skoglundh, H. Härelind, Catal. Today (2014), Accepted for publication http://dx.doi.org/10.1016/j.cattod.2014.11.029
[37] K. Shimizu, K. Sawabe, A. Satsuma, Catal. Sci. Technol. 1 (2011) 331–341.
[38] H. Kannisto, H.H. Ingelsten, M. Skoglundh, Top. Catal. 52 (2009) 1817–1820.
[39] S.T. Korhonen, A.M. Beale, M.A. Newton, B.M. Weckhuysen, J. Phys. Chem. C 115 (2011) 885–896.
[40] R. Burch, J.P. Breen, C.J. Hill, B. Krutzsch, B. Konrad, E. Jobson, L. Cider, K. Eranen, F. Klingstedt, L.E. Lindfors, Top. Catal. 30–31 (2004) 19–25.
[41] B. Wichterlova, P. Sazama, J.P. Breen, R. Burch, C.J. Hill, L. Capek, Z. Sobalik, J. Catal. 235 (2005) 195–200.
[42] S. Chansai, R. Burch, C. Hardacre, J. Breen, F. Meunier, J. Catal. 276 (2010) 49–55.
[43] S. Tamm, N. Vallim, M. Skoglundh, L. Olsson, J. Catal. 307 (2013) 153–161.
[44] C. Thomas, Appl. Catal. B 162 (2015) 454–462.
[45] R. Brosius, K. Arve, M.H. Groothaert, J.A. Martens, J. Catal. 231 (2005) 344–353.
[46] M. Andersson, J.S. Pedersen, A.E.C. Palmqvist, Langmuir 21 (2005) 11387–11396.
[47] J.W. Chorkendorff, Concepts of Modern Catalysis and Kinetics, Wiley-VCH GmbH & Co. KGaA, 2003, pp. 185–190.
[48] M. Männikkö, M. Skoglundh, H.H. Ingelsten, Appl. Catal. B 119–120 (2012) 256–266.
[49] S. Tamm, H.H. Ingelsten, M. Skoglundh, A.E.C. Palmqvist, J. Catal. 276 (2010) 402–411.
[50] T. Chaieb, L. Delannoy, C. Louis, C. Thomas, Appl. Catal. B 142 (2013) 780–784.
[51] Y.M. Luo, J.M. Hao, Z.Y. Hou, L.X. Fu, R.T. Li, P. Ning, X.M. Zheng, Catal. Today 93–5 (2004) 797–803.
[52] A.N. Pestryakov, A.A. Davydov, J. Electron Spectrosc. Relat. Phenom. 74 (1995) 195–199.
[53] A. Keshavaraja, X. She, M. Flytzani-Stephanopoulos, Appl. Catal. B 27 (2000) L1–L9.
[54] A. Musi, P. Massiani, D. Brouri, J.M. Trichard, P. Da Costa, Catal. Lett. 128 (2009) 25–30.
[55] K. Arve, L. Capek, F. Klingstedt, K. Eranen, L.E. Lindfors, D.Y. Murzin, J. Dedecek, Z. Sobalik, B. Wichterlova, Top. Catal. 30–31 (2004) 91–95.
[56] K. Sato, T. Yoshinari, Y. Kintaichi, M. Haneda, H. Hamada, Appl. Catal. B 44 (2003) 67–78.
[57] I.H. Son, M.C. Kim, H.L. Koh, K.L. Kim, Catal. Lett. 75 (2001) 191–197.
[58] A. Iglesias-Juez, A.B. Hungria, A. Martinez-Arias, A. Fuerte, M. Fernandez-Garcia, J.A. Anderson, J.C. Conesa, J. Soria, J. Catal. 217 (2003) 310–323.
[59] G.A. Ozin, H. Huber, Inorg. Chem. 17 (1978) 155–163.
[60] L. Zhang, C.B. Zhang, H. He, J. Catal. 261 (2009) 101–109.
[61] E. Sayah, D. Brouri, P. Massiani, Catal. Today 218 (2013) 10–17.
[62] J.J. Mock, M. Barbic, D.R. Smith, D.A. Schultz, S. Schultz, J. Chem. Phys. 116 (2002) 6755–6759.
[63] E. Sayah, D. Brouri, Y.H. Wu, A. Musi, P. Da Costa, P. Massiani, Appl. Catal. A 406 (2011) 94–101.
[64] M.K. Kim, P.S. Kim, J.H. Baik, I.S. Nam, B.K. Cho, S.H. Oh, Appl. Catal. B 105 (2011) 1–14.
[65] G. Busca, Catal. Today 27 (1996) 457–496.
[66] K. Shimizu, M. Tsuzuki, K. Kato, S. Yokota, K. Okumura, A. Satsuma, J. Phys. Chem. C 111 (2007) 950–959.
[67] T.P. Beebe, J.E. Crowell, J.T. Yates, J. Phys. Chem. 92 (1988) 1296–1301.
[68] V.A. Matyshak, L.A. Berezina, O.N. Sil'chenkova, V.F. Tret'Yakov, G.I. Lin, A.Y. Rozovskii, Kinet. Catal. 50 (2009) 111–121.
[69] A.R. McInroy, D.T. Lundie, J.M. Winfield, C.C. Dudman, P. Jones, D. Lennon, Langmuir 21 (2005) 11092–11098.
[70] A. Nagy, G. Mestl, T. Ruhle, G. Weinberg, R. Schlogl, J. Catal. 179 (1998) 548–559.
[71] V.A. Matyshak, L.A. Berezina, O.N. Sil'chenkova, V.F. Tret'yakov, G.I. Lin, A.Y. Rozovskii, Kinet. Catal. 50 (2009) 255–263.
[72] N. Bion, J. Saussey, M. Haneda, M. Daturi, J. Catal. 217 (2003) 47–58.
[73] F. Thibault-Starzyk, E. Seguin, S. Thomas, M. Daturi, H. Arnolds, D.A. King, Science 324 (2009) 1048–1051.
[74] S. Chansai, R. Burch, C. Hardacre, D. Norton, X. Bao, L. Lewis, Appl. Catal. B 160 (2014) 356–364.
[75] R. Matarrese, H.H. Ingelsten, M. Skoglundh, J. Catal. 258 (2008) 386–392.
[76] H. Knozinger, P. Ratnasamy, Catal. Rev. Sci. Eng. 17 (1978) 31–70.
[77] G. Busca, V. Lorenzelli, V.S. Escribano, R. Guidetti, J. Catal. 131 (1991) 167–177.
[78] T.H. Ballinger, J.T. Yates, Langmuir 7 (1991) 3041–3045.
[79] J.G. Chen, P. Basu, T.H. Ballinger, J.T. Yates, Langmuir 5 (1989) 352–356.